

# A systematic simulation of the effect of salicylic acid on sphingolipid metabolism

Chao Shi, Jian Yin, Zhe Liu, Jian-Xin Wu, Qi Zhao, Jian Ren and Nan Yao\*

State Key Laboratory of Biocontrol, Guangdong Key Laboratory of Plant Resources, School of Life Sciences, Sun Yat-sen University, Guangzhou 510275, P. R. China

\*Correspondence: Nan Yao, State Key Laboratory of Biocontrol, Guangdong Key Laboratory of Plant Resources, School of Life Sciences, Sun Yat-sen University, Guangzhou 510275, P. R. China  
yaonan@mail.sysu.edu.cn

**Keywords:** Ceramides<sub>1</sub>, Salicylic acid<sub>2</sub>, Sphingolipid<sub>3</sub>.

## Abstract:

The phytohormone salicylic acid (SA) affects plant development and defense responses. Recent studies revealed that SA is also involved in the regulation of sphingolipid metabolism, but the details of this regulation remain to be explored. Here, we use *in silico* Flux Balance Analysis (FBA) with published microarray data to construct a whole-cell simulation model, including 23 pathways, 259 reactions and 172 metabolites, to predict the alterations in flux of major sphingolipid species after treatment with exogenous SA. This model predicts significant changes in fluxes of certain sphingolipid species after SA treatment, changes that likely trigger downstream physiological and phenotypic effects. To validate the simulation, we used isotopic non-stationary metabolic flux analysis to measure sphingolipid contents and turnover rate in *Arabidopsis thaliana* seedlings treated with SA or the SA analog benzothiadiazole (BTH). The results show that both SA and BTH affect sphingolipid metabolism by not only concentration of certain species, but also the optimal flux distribution and turnover rate of sphingolipid contents. Our strategy allows us to formally estimate sphingolipid fluxes on a short time scale and gives us a systemic view of the effect of SA on sphingolipid homeostasis.

## 33 INTRODUCTION

34 Salicylic acid (SA), an important phenolic phytohormone, has well-known roles in  
35 pathogen-triggered defense responses including microbe-associated molecular pattern-triggered  
36 immunity, effector-triggered immunity, and systemic acquired resistance (Jones and Dangl, 2006;  
37 Spoel and Dong, 2012; Yan and Dong, 2014). SA also participates in abiotic stress responses  
38 (Vlot *et al.*, 2009; Miura and Tada, 2014) and in plant development, including vegetative and  
39 reproductive growth (Vicente and Plasencia, 2011). SA also has indispensable functions in the  
40 maintenance of redox homeostasis (Durner and Klessig, 1995 & 1996; Slaymaker *et al.*, 2002)  
41 and respiratory pathways (Moore *et al.*, 2002). The SA analog benzothiadiazole (BTH) activates  
42 the SA signaling pathway, triggers expression of defense genes (Shimono *et al.*, 2007), and shows  
43 similar physiological effects to SA (Lawton *et al.*, 1996).

44 As a key mediator of defense response, the SA pathway crosstalks with many metabolic pathways.  
45 Sphingolipids are a family of complex lipids that have a serine-based head, a fatty acyl chain, and  
46 a long-chain base (LCB). Covalent modifications and variability in the length of the fatty acyl  
47 chain increase sphingolipid diversity. Sphingolipids are important structural and functional  
48 components of the plasma membrane (Hannun and Obeid, 2008) and have important functions in  
49 the plant immune response, abiotic stress responses, and developmental regulation (Chen and  
50 Cahoon, 2009; Pata *et al.*, 2009; Markham *et al.*, 2013; Bi *et al.*, 2014). In *Arabidopsis*, ceramides,  
51 a group of sphingolipids, affect SA-mediated defense responses and programmed cell death  
52 (PCD). Some mutants in the sphingolipid metabolic pathway show high levels of expression of  
53 defense-related genes, accumulate SA, and undergo PCD. The ceramide kinase deficient mutant  
54 *accelerated cell death 5 (acd5)* accumulates SA and ceramides late in development, but shows  
55 increased susceptibility to pathogens (Greenberg *et al.*, 2000; Liang *et al.*, 2003; Bi *et al.*, 2014).  
56 Wang *et al.* (2008) reported that the insertion knock out mutant of *Arabidopsis*  
57 inositolphosphorylceramide synthase 2 (*erh1*) also spontaneously accumulates SA. Similar  
58 increases in SA levels have also been observed in mutants of the sphingosine transfer protein  
59 mutant *acd11* (Brodersen *et al.*, 2002), the *Arabidopsis* sphingolipid fatty acid hydroxylase  
60 mutants *fah1 fah2* (Konig *et al.*, 2012), and *mips1* (D-myo-inositol 3-phosphate synthase 1)  
61 mutants (Meng *et al.*, 2009). Moreover, SA accumulation and PCD signaling mediated by MAPK  
62 affect the levels of free LCB (Saucedo-Garcia *et al.*, 2011). However, *fah1 fah2* mutants  
63 accumulate SA and have moderate levels of LCB (Konig *et al.*, 2012). Thus, the SA and  
64 sphingolipid pathways have significant but complex crosstalk, particularly in defense and cell  
65 death.

66 Metabolic modeling performs well in prediction of physiological changes and metabolic  
67 outcomes resulting from genetic manipulation, where changes in metabolite levels have a strong  
68 effect on cellular behavior (Smith and Stitt 2007; Stitt *et al.*, 2010). The genome of *Arabidopsis*  
69 *thaliana* has been sequenced, making whole-genome metabolic reconstruction feasible (Thiele

70 and Palsson, 2010; Seaver *et al.*, 2012). Much of the early modeling work used steady-state  
71 Metabolic Flux Analysis (MFA), based on a steady-state model of the plant metabolic network,  
72 and on experiments using isotope labeling to trace metabolites of interest (Libourel and  
73 Shachar-Hill, 2008; Allen *et al.*, 2009; Kruger *et al.*, 2012). This method provided insights on  
74 metabolic organization and modes, but has difficulties in labeling heterotrophic tissues  
75 (Sweetlove and Ratcliffe, 2011), over-relies on manual curation of metabolic pathways  
76 (Masakapalli *et al.*, 2010; Sweetlove and Ratcliffe, 2011; Kruger *et al.*, 2012), and uses  
77 low-throughput detection, making systematic analysis difficult (Lonien and Schwender, 2009;  
78 Sweetlove and Ratcliffe, 2011).

79 By contrast, Flux Balance Analysis (FBA) overcomes many of the drawbacks of MFA. In FBA, a  
80 model is established based on a group of ordinary differential equations that formulate a transient  
81 quasi-steady state of the metabolic fluxome of target pathways. The duration of the transient  
82 flux balance calculated by the FBA model is almost negligible compared to the long-term,  
83 fundamental metabolic changes that occur during development or environmental responses  
84 (Varma and Palsson, 1994). In addition, FBA does not require isotopic labeling, suits a variety of  
85 trophic modes, and is more flexible than steady-state MFA in handling groups of flux distributions  
86 by linear programming and other methods for optimization under constraints (Edward and  
87 Palsson, 2000; Reed and Palsson, 2003). Several *Arabidopsis* metabolic models based on FBA are  
88 available online (Poolman *et al.*, 2009; Dal'Molin *et al.*, 2010; Radrich *et al.*, 2010).

89 Apart from FBA simulation, fluxomic changes can also be directly measured. Derived from  
90 steady-state MFA, isotopic non-stationary metabolic flux analysis (INST MFA) measures *in vivo*  
91 time-courses of the transient patterns of isotopic labeling and the steady-state concentrations of  
92 various metabolites. Compared with its predecessor, INST MFA has specific advantages, as it is  
93 rapid, can deal with monolabeled metabolites (Shastri *et al.*, 2007), can directly measure each flux  
94 (Wiechert and Nöh, 2005), and can validate flux predictions made by either laboratory or  
95 computational analyses (Nöh and Wiechert, 2006 & 2011; Noack *et al.* 2010).

96 Since metabolic changes substantially affect the crosstalk between SA and sphingolipids, in this  
97 study we constructed a metabolic model to simulate SA-related changes in the sphingolipid  
98 pathway. We constructed an *Arabidopsis* whole-cell FBA model including 23 pathways, 259  
99 reactions and 172 metabolites. Based on their relative enrichment and responsiveness to SA  
100 stimulation, our model includes 40 sphingolipid species, comprising LCBs, ceramides,  
101 hydroxyceramide and glucosylceramides. Due to the lack of flux data on plant sphingolipid  
102 metabolism, we used <sup>15</sup>N labeled INST MFA to measure sphingolipid flux in untreated plants and  
103 calibrate the FBA model. After that, additional expression profiles from plants treated with SA  
104 and BTH (a SA analog) were supplied to the model. The FBA model was then calculated *in silico*  
105 for the prediction and comparison of the optimal flux distribution and flux variability in SA- and  
106 BTH-treated and untreated conditions. We then used INST MFA with <sup>15</sup>N-labeled samples to

107 measure the flux changes directly. Both the computational model and the experiments showed  
108 consistent and significant changes in the sphingolipid pathway in response to SA and BTH. Our  
109 data gives us a systemic view of the effect of SA on sphingolipid homeostasis.

110

111

## 112 **MATERIALS AND METHODS**

113

### 114 **Plant materials**

115 Wild type *Arabidopsis thaliana* ecotype Columbia seedlings were grown vertically on 1/2x  
116 Murashige & Skoog (MS) medium for 10 days after 2-day vernalization. The culture dishes were  
117 incubated at 22 °C under a 16 h light/8 h dark cycle. For labeling the plant seedlings in liquid  
118 medium, the culture dishes were incubated at 22 °C with 24 h light.

119

### 120 **Labeling and treatments**

121 The different sphingolipids have many carbon atoms in different positions; therefore, labeling the  
122 only nitrogen in the serine-based head group would be much easier for LC-MS/MS measurements.  
123 Thus, we used <sup>15</sup>N serine (Cambridge Isotope Laboratories, Inc. MA, USA) in the labeling  
124 experiment. Ten-day-old seedlings were transferred to N-deficient 1/2x MS liquid medium  
125 (Yoshimoto *et al.*, 2004) in 12-well culture plates. 5 mM <sup>15</sup>N-labelled serine was supplied to  
126 compensate for the shortage of nitrogen (Hirner *et al.*, 2006) and used as the only source of  
127 isotope. For SA and BTH treatments, 100 μM SA or 100 μM BTH was supplied to the labeling  
128 medium. The seedlings were treated or not treated for 0, 1, 3, 5, 7, 9, and 24 hours for isotopic  
129 non-stationary transient labeling (Nöh and Wiechert, 2006) before sphingolipid extraction.

130

### 131 **Experimental measurement of turnover rate**

132 Since serine has only one nitrogen atom and each sphingolipid has only one serine, the fraction of  
133 each labeled sphingolipid species can be simply measured as:

$$134 \text{ } ^{15}\text{N fraction}\% = \frac{^{15}\text{N}}{\text{N}} * 100$$

135 Where <sup>15</sup>N is the concentration of <sup>15</sup>N labeled molecules of a specific sphingolipid species, and N  
136 is the total concentration of that sphingolipid species, whether labeled or not.

137 The turnover rate of a sphingolipid species is calculated from the slope of the curve of the  
138 time-course of <sup>15</sup>N incorporation from the initial time that the fraction begins to increase to the  
139 fraction stabilizes. Also, the isotopic incorporation rate r can be calculated as:

$$140 r = \frac{d \text{ } ^{15}\text{N fraction}}{dt} * \text{N}$$

141

142 In the measurement, the natural enrichment of  $^{15}\text{N}$  is relatively constant between samples and  
143 treatments.

#### 144 **Sphingolipid measurements**

145 The plants cultured in labeling medium for the time periods described above were weighed and  
146 metabolically quenched by freezing in liquid nitrogen. Sphingolipid species were then extracted  
147 and measured by LC-MS/MS as described by Bi *et al.* (2014) with a slight modification to cope  
148 with isotopic-labeled sphingolipid species. Major sphingolipid species were subsequently  
149 analyzed with a Shimadzu 20A HPLC tandem AB SCIEX TripleTOF 5600<sup>+</sup> mass spectrometer.  
150 The sphingolipid species were analyzed using the software Multiquant (AB SCIEX)

151

#### 152 **Metabolic model construction**

153 The *Arabidopsis* whole-cell metabolic model was constructed with 23 pathways, 259 reactions,  
154 and 172 metabolites. Primary metabolic pathways refer to the KEGG (Kyoto Encyclopedia of  
155 Genes and Genomes <http://www.genome.jp/kegg/>, Kanehisa *et al.*, 2008), AraCyc database  
156 (Mueller *et al.*, 2003), and AraGEM model (Dal'Molin *et al.*, 2010), with manual curation for  
157 sphingolipid metabolism, including major ceramide, hydroxyceramide, and glucosylceramide  
158 species (Table S1). We used biomass as the objective function with the stoichiometries of major  
159 components were assigned to their biomass fraction, which comprises major carbohydrates,  
160 amino acids and lipids, according to experiments or the literature (Fiehn *et al.*, 2000; Welte *et al.*,  
161 2002; Dal'Molin *et al.*, 2010). For sphingolipid species, the objective function stoichiometries  
162 were set to the adjusted isotopic incorporation rate in labeling experiments.

163

#### 164 **Flux balance analysis (FBA)**

165 Flux balance modeling uses a group of ordinary differential equations. The analysis requires a  
166 stoichiometric matrix ( $S$ ) and a vector ( $v$ ) built for each reaction, where  $s_{ij}$  in the  $S$  matrix is the  
167 stoichiometric number of the  $i$ th metabolite in the  $j$ th reaction and  $v_j$  is the rate of the  $j$ th reaction,  
168 which is subjected to upper and lower boundary constraints. To reach the *in silico* “quasi-steady  
169 state”, the following condition must be fulfilled:

$$170 \quad S \cdot v = 0$$

171 After solving the FBA equation with the constraints above (Edwards and Palsson, 2000; Edwards  
172 *et al.*, 2001), a linear-programming optimization method (Edwards and Palsson, 2000) was  
173 applied to pick the most plausible (groups of) flux distributions among the solution space  
174 according to the objective setting.

175

## 176 *in silico* SA and BTH treatments

177 To incorporate the effect of exogenous SA and BTH on the wild-type plant into the model, we  
178 used published microarray data for SA- and BTH-treated *Arabidopsis* (for SA, Leeuwen *et al.*,  
179 2007; for BTH, Wang *et al.*, 2006). We assumed that the metabolic flux changed following the  
180 same trend as the respective gene expression levels. Therefore, when genes were matched to  
181 microarray probes to identify their changes in expression following each treatment, we picked  
182 genes that changed more than 1.5-fold in SA-treated plants and more than 2-fold in BTH-treated  
183 plants (Table S2). Then, the adjusted model was recalculated for optimal flux distribution.

184

## 185 Flux variability analysis (FVA)

186 The stoichiometry model is a self-balancing model in that any flux distributions that fulfill the  
187 constraints are involved in its solution space. Through the sampling of the solution space or  
188 sensitivity analysis, each reaction is tested for its possible upper flux limit and lower flux limit  
189 under constraints (Mahadevan and Schilling, 2003). The calculated range of each flux is an  
190 important indicator of the role of the corresponding reaction in the robustness of the whole  
191 network. To make a physiologically relevant estimation, we sample the flux space which achieves  
192 at least 80% of optimal objective rate (in our model, the biomass production) under untreated or  
193 treated condition.

194

## 195 Simulation environment

196 The model of *Arabidopsis* was built in SBML (Systems Biology Markup Language) (Hucka *et al.*,  
197 2003) in XML format. SBML Toolbox 2.0.2 (Keating *et al.*, 2006; Schmidt and Jirstrand, 2006)  
198 and COBRA Toolbox 2.0.5 (Schellenberger *et al.*, 2011) in MATLAB 2012a (Mathworks Inc.;  
199 Natick, MA) were used for model construction and calculation. Linear programming was  
200 performed with GLPK (GNU Linear Programming Kit, <http://www.gnu.org/software/glpk/>). The  
201 rank-test and multiple covariance analysis are performed using IBM SPSS Statistics 19 (IBM  
202 Corp. Released 2010. IBM SPSS Statistics for Windows, Version 19.0. Armonk, NY: IBM Corp.).

203

204

## 205 RESULTS

206

### 207 Model construction for plant sphingolipid metabolism

208 We aimed to explore the changes in plant sphingolipid metabolism in response to SA, by using

209 computational modeling and experiments. Although sphingolipids function as important  
210 components in plant development and stress responses, their metabolism remains obscure, with  
211 few measured network parameters. FBA is well suited to the simulation of a metabolic fluxome  
212 with poorly-understood dynamics (Varma and Palsson, 1994), as FBA requires only the  
213 stoichiometric relationship in each reaction and the objective function for optimization. In our  
214 model, the numbers of molecules of reactants and products in known reactions were obtained  
215 from public databases (see Materials and Methods). For the sphingolipid pathways (Table S1),  
216 those reactions that have not been determined were inferred from their atomic composition or  
217 similar reactions. Considering that metabolic balances are mainly affected by a few metabolites  
218 that are either in a hub of the network or have high turnover, we picked the sphingolipid species  
219 that are relatively abundant or central to the known network (Table 1). Since  
220 inositolphosphorylceramide and its derivatives are difficult to measure in plants, we excluded  
221 those species from our model.

222

### 223 **Isotopic non-stationary transient labeling of sphingolipids**

224 To inform the objective function and to validate the model's prediction, we used the *in vivo*  
225 fluxomic method of isotopic non-stationary transient labeling (INST) to directly measure the  
226 turnover rate of plant sphingolipids. In previous work,  $^{13}\text{C}$  INST was mostly used to examine  
227 central pathways such as glucose metabolism or photosynthesis (Noack *et al.*, 2010; Nöh and  
228 Wiechert, 2011), where limited numbers of labeled fragments are detected by mass spectrometry.  
229 However, the simplest sphingolipid has at least 18 carbon atoms, and their combined transitions,  
230 modifications and fragmentation would generate large numbers of labeled fragments; therefore  
231 mass spectrometry quantification of  $^{13}\text{C}$  labeled sphingolipid would be extremely difficult,  
232 whatever the labeling material used. Therefore, we selected the only nitrogen atom in the head of  
233 each sphingolipid as the labeling position. To distinguish between artificial and natural  $^{15}\text{N}$ , we  
234 measured the composition of natural  $^{15}\text{N}$  sphingolipid in unlabeled samples, finding different  
235 levels of natural  $^{15}\text{N}$  in each sphingolipid species. This fraction is constant between measurements  
236 and treatments in each species, and thus cannot affect the comparison of isotopic incorporation  
237 rates between experiments.

238 We transiently labeled 10-day-old seedlings in a time course. The isotopic incorporation curves  
239 (see representative species shown in Figure 1) reveal that the labeled serine is absorbed and  
240 incorporated into sphingolipid in the first hour of labeling, followed by a uniform turnover rate.  
241 For LCB (Figure 1D), ceramide (Figure 1A), and hydroxyceramide species (Figure 1B), the  
242 isotopic incorporation curves gradually flatten and finally reach an isotopic fraction balance  
243 between 9 and 24 h. A noticeable, small drop occurs around the 5<sup>th</sup> hour of incorporation in LCB  
244 (Figure 1D). The incorporation of  $^{15}\text{N}$  in these simple sphingolipids is fast, and the final balanced

245 isotopic fraction can reach 40-65% (Figure 1A, 1B and 1D). By contrast, between 9 and 24 h, the  
246 labeled fraction constantly rose for the glucosylceramides (Figure 1C), which had a lower rate of  
247 incorporation than the ceramides or hydroxyceramides. Combined with the concentration of  
248 sphingolipids, we calculated the isotopic incorporation rate as shown in Table 2.

249

## 250 **Flux balance analysis (FBA) of the flux distribution in untreated plants**

251 The objective function in the FBA model guides flux determination by simulating a transient flux  
252 distribution. However, biomass at a certain time is the complex result of development through the  
253 organism's entire life, and hence cannot be a relevant principle in setting the objective function in  
254 our model of the *Arabidopsis* seedling. Instead, the objective function stoichiometries of the  
255 sphingolipid pathway was built and adjusted from isotopic incorporation rates in the above  
256 labeling experiments (Table 1). Then, flux balance optimization was performed. Figure 2 shows  
257 the simulated flux distributions of sphingolipid species in untreated plants.

258

259 The simulation data in Figure 2 shows that LCBs, very-long-chain ceramides and  
260 hydroxyceramides compose the highest fraction of total flux. The <sup>15</sup>N labeled INST MFA is  
261 consistent with these simulated results for the measured fast isotopic incorporation and high  
262 fraction of stabilized isotopic final level of LCB, ceramides and hydroxyceramides (Figure 1).  
263 These results demonstrate that LCBs, the sphingolipids that have the smallest pool size, also have  
264 the highest turnover among plant sphingolipids. Very-long-chain ceramides and  
265 hydroxyceramides are important not only for their hub position connecting glucosylceramides and  
266 sphingosine, but also carry a huge flux throughput in sphingolipid turnover and thus help maintain  
267 sphingolipid homeostasis. Both the simulation and experimental results indicate that these  
268 sphingolipid species are probably more responsive to disturbance, and thus are frequently used by  
269 pathogens to manipulate or interfere with host sphingolipid metabolism (Asai *et al.*, 2000;  
270 Markham *et al.*, 2011, Bi *et al.*, 2014).

271

272 Although the glucosylceramides have much larger pool sizes (Table 1) than the ceramides,  
273 hydroxyceramides, or LCBs, they have smaller metabolic fluxes than their precursors (Figure 2).  
274 These results are validated by the slow but lasting incorporation of isotope into glucosylceramide  
275 pools (Figure 1C). The relatively slow turnover is in accordance with the function of  
276 glucosylceramides as membrane structural components, indicating a slow but continuous  
277 accumulation in the cell membrane during plant development. The accordance of simulation and  
278 experiment results also supports our choice of objective function stoichiometries setting, for the  
279 scale of simulated and measured sphingolipid metabolic flux distribution (Figure 2 and Table 2) is  
280 nearly unrelated to the distribution of sphingolipid biomass (Table 1).

281



282 ***In silico* SA and BTH treatments**

283 The FBA model hypothesizes the quasi-steady state condition of the target network, and we  
284 assume that the sphingolipid pathway will reach at least a transient metabolic balance after SA  
285 treatment. Thus, we employed the previous model simulating the resting state to predict the  
286 effects of SA treatment. We first used data from microarray analysis of SA- and BTH-treated  
287 plants to simulate the effect of these treatments on sphingolipid flux. Sphingolipid-related genes  
288 were chosen (see Method) from two microarrays (Table S2). *LAG 1 HOMOLOG 2 (LOH2)*,  
289 which encodes a ceramide synthase (Brandwagt *et al.*, 2000; Ternes *et al.*, 2011), shows the  
290 highest up-regulation after both SA and BTH treatments, and other genes show different  
291 expression between treatments (*SPHINGOID BASE HYDROXYLASE 2 (SBH2)*, *FATTY*  
292 *ACID/SPHINGOLIPID DESATURASE (SLD)*, *FATTY ACID HYDROXYLASE 2 (FAH2)*,  
293 *SPHINGOSINE-1-PHOSPHATE LYASE (AtDPL1)*). The reactions regulated by the genes with  
294 altered transcript levels were then picked for incorporation in the model. The flux boundaries of  
295 these reactions were altered based on the gene expression level, and the adjusted model was  
296 recalculated for flux balance analysis.

297 Compared with the model simulating the resting state, *in silico* SA and BTH treatments resulted  
298 in a nearly three-fold increase of flux in long-chain ceramide species (Figure 2), which is  
299 consistent with the up-regulation of *LOH2* in the microarray data. In particular, simulated SA and  
300 BTH treatment both showed a significant rise in metabolism of trihydroxy glucosylceramides.  
301 This increase is not specific to fatty acid species, which showed an increase in both trihydroxy  
302 long-chain and very-long-chain glucosylceramides (Figure 2). These results are consistent with  
303 the data from <sup>15</sup>N labeled INST MFA (Table 2). Interestingly, the microarray data showed no  
304 significant changes in genes that directly catalyze the pathways in glucosylceramide metabolism,  
305 nor any related to glucosylceramide, in response to SA or BTH treatment (Table S2). Considering  
306 the down-regulation of *SBH2* under BTH treatment, we believe that the increase of  
307 glucosylceramide metabolism may mainly be induced by the upstream up-regulation of *LOH2*.  
308 Since the increase of the turnover rate is not linked to metabolite concentration, the changes of  
309 glucosylceramides are almost negligible by typical quantitative LC-MS/MS measurement, but the  
310 increase in lipid renewal may have indispensable functions in the sensitivity of membrane-based  
311 cell signaling.

312 In this simulation, although some genes change differently in response to SA and BTH treatment  
313 (Table S2), they have similar effects on sphingolipid metabolism. Our model also proposes a  
314 possible mechanism by which BTH affects the network under flux balance constraint without  
315 mimicking all the gene expression changes of its counterpart.

316

## 317 **Isotopic non-stationary transient measurement of the effect of SA and BTH**

318 Last, to confirm the predictions of the model, we directly measured the *in vivo* flux change in  
319 response to SA and BTH treatments. For SA and BTH treatments, the isotope incorporation rate  
320 significantly increased for certain sphingolipid species such as LCBs and ceramides (Table 2).  
321 These results are consistent with our FBA model (Figure 2).

322

## 323 **Flux variability analysis**

324 To examine the change in network rigidity in response to SA and BTH treatments, we estimated  
325 the accessible flux ranges of sphingolipid species *in silico*. To make a physiologically relevant  
326 estimation, we sampled the flux space which achieves at least 80% of optimal objective rate (in  
327 our model, the biomass production) under untreated or treated condition. We sorted the flux range  
328 into three types (Oberhardt *et al.*, 2010): rigid flux (flux range near zero but with non-zero flux  
329 value), bounded flexible flux, and infinitely flexible flux (boundary spans from 0 or -1000 to 1000  
330 in the model). In the fluxome of treated and untreated plants, LCB fluxes were infinitely flexible,  
331 showing a high capacity to tolerate disturbance, ceramide and glycosylceramide fluxes showed  
332 bounded flexibility, and hydroxyceramide fluxes were rigid (Table S3). The limited flux  
333 variability of most sphingolipids is consistent with stoichiometric modeling result in *S. cerevisiae*  
334 (Ozbayraktar and Ulgen, 2011). Similar with isotopic incorporation experiments, we found the  
335 disturbances of flux variability in the reaction of ceramide and glucosylceramide metabolic fluxes  
336 after SA and BTH treatments (Figure 3), indicating freedom of adjusting their metabolism under  
337 the prerequisite of sphingolipid flux homeostasis during defense process.

338

339

## 340 **DISCUSSION**

341 Our FBA model and isotope labeling experiments systematically explored the alterations in the  
342 sphingolipid pathway that occur in response to SA and BTH. It is well-known that traditional  
343 metabolic responses are often considered to be significant changes of certain metabolites  
344 concentration. However, the systematic responses caused by plant activator and phytohormone  
345 cannot be achieved by only doubling the concentration fold of certain nodes without affecting the  
346 dynamic properties of the whole network. To panoramically detect these underlying changes of  
347 network parameters presented by up and down of certain nodes, one of the most direct  
348 measurements is the fluxome. FBA analysis has been applied in microbial metabolic engineering  
349 and modeling of other systems. However, construction of the model for sphingolipid metabolism  
350 presented difficulties related to the unique features of sphingolipid pathways. Although  
351 sphingolipid species are among the most reactive components in plant development and stress

352 responses, they reside in the periphery of the network of plant metabolism, having loose  
353 metabolic connections with other subnetworks. Their lack of connection and remote position  
354 make the flux in the self-balanced function more susceptible to the objective settings, rather than  
355 being affected by artificial constraints and neighboring subnetworks.

356 Indeed, there are other studies concerning sphingolipids in *S. cerevisiae* (Ozbayraktar and Ulgen,  
357 2011) where the sphingolipid pathways are also remote from central metabolism, but these  
358 models are backed by experimental data on enzyme kinetic parameters or known fluxes. In  
359 experiments, plant sphingolipid pathways are difficult to explore because of their vast diversity,  
360 low abundance, and lack of sensitive and replicable measurements. In addition, the enzymes  
361 linking metabolites often are embedded in the layers of membranes, making the isolation and  
362 estimation of their kinetic properties difficult. Until now, a limited set of experiments has  
363 determined only a rough scheme of plant sphingolipid metabolism. Considering that, we used the  
364 experimentally measured isotopic incorporation rate to set the stoichiometry of each sphingolipid  
365 species as stoichiometries in the objective function, and we found that the resulting flux  
366 distribution of each species is in accordance with isotopic incorporation pattern, demonstrating  
367 that isotopic incorporation data produces a better fit than biomass fraction in objective  
368 stoichiometry determination, as the maximization of biomass is often considered as the aim of  
369 plant metabolism regardless of any inconsistency between biomass contents and generation  
370 rate of each component.

371 In the experimental part, isotopic transient labeling provided a direct measurement of *in vivo* flux.  
372 We note that none of the sphingolipid species reached 100% labeled. Similar phenomena were  
373 also observed in other experiments (Delwiche and Sharkey, 1993; Hasunuma *et al.*, 2010).  
374 Considering the internal serine sources and anaplerotic reactions of complex existing  
375 sphingolipids, the pattern indicates a balance of labeled and unlabeled sphingolipids in the  
376 metabolic pool. Since the only exogenous source of nitrogen is labeled, we can also speculate on  
377 the utilization of external and internal sources of nitrogen in sphingolipid synthesis from the  
378 isotopic incorporation curve.

379 There are various models linking plant sphingolipid pathways with hormones and their synergistic  
380 role in plant development and stress responses. In these models, the possible sphingolipid  
381 inducers of defense responses include LCBs (Saucedo-García *et al.*, 2011) and ceramides  
382 (Markham *et al.*, 2011, Bi *et al.*, 2014), with SA both up- and downstream of  
383 sphingolipid-mediated PCD (Saucedo-García *et al.*, 2011; Bi *et al.*, 2014). As sphingolipid  
384 mutants often accumulate SA, the effect of SA on ceramide species may include positive feedback  
385 on the imbalance of sphingolipids. Our results are in accordance with the observed frequent  
386 variation in the concentration of LCB and sometimes ceramide, but less variation in the  
387 concentrations of hydroxyceramide and glucosylceramide in wild-type *Arabidopsis*. Functionally  
388 speaking, since LCB and ceramides are fundamental to sphingolipid metabolism and show high

389 flux flexibility, they can be more responsive to stimuli such as SA or BTH without disrupting the  
390 total fluxomic balance of sphingolipid metabolism

391  
392 In a living cell, the synthesis and degradation of all substances occurs through metabolism.  
393 However, current research tends to separate metabolites and functional molecules. The most  
394 exciting aspect of plant sphingolipids is that they are themselves metabolites and functional  
395 molecules. Our current model only deals with their metabolic properties in a self-balanced manner.  
396 It will be interesting to incorporate the signaling network that involves sphingolipids to build an  
397 integrated model to consider the direct effect of metabolism on cell signaling.

398

## 399 CONCLUSION

400 In this study, we established a sphingolipid FBA model and used  $^{15}\text{N}$  labeled isotopic transient  
401 labeling to systematically explore the effects of SA and BTH on sphingolipid metabolic pathways.  
402 The results show increases in ceramide and glucosylceramide flux in response to exogenous SA  
403 and BTH and also alteration of their flux variability. Our results also give us insights that help  
404 explain the mechanism of crosstalk between SA and sphingolipids, and their roles in the plant  
405 defense response.

406

407

## 408 ACKNOWLEDGEMENT

409 We thank members in the Yao and Ren laboratories for assistance with this work. This work was  
410 supported by the National Key Basic Science 973 Program (2012CB114006), National Natural  
411 Science Foundation of China (31170247), and the Fundamental Research Funds for the Central  
412 Universities (13lgjc27).

413

## 414 Supplemental information:

415

416 **Table S1.** The indexes, categories and equations of sphingolipid-related reactions in our FBA  
417 model.

418

419 **Table S2.** Sphingolipid-related gene expression changes in SA- and BTH-treated plants from  
420 microarrays data published by van Leeuwen *et al.* (2007) and Wang *et al.* (2006).

421

422 **Table S3.** Simulated flux variability of sphingolipid-related reactions in untreated and *in silico*

423 SA- or BTH- treated plants.

424

425

426

## 427 REFERENCES

428

429 Allen, D.K., Libourel, I.G.L. and Shachar-Hill, Y. (2009). Metabolic flux analysis in plants: coping with complexity.

430 *Plant Cell Environ.* 32, 1241-1257.

431

432 Bi, F-C., Liu, Z., Wu, J-X., Liang, H., Xi, X-L., Fang, C., Sun, T-J., Yin, J., Dai, G-Y., Rong, C., Greenberg, J.T., Su,

433 W-W. and Yao, N. (2014). Loss of ceramide kinase in *Arabidopsis* impairs defenses and promotes ceramide

434 accumulation and mitochondrial H<sub>2</sub>O<sub>2</sub> bursts. *Plant Cell.* 26, 3449-3467.

435

436 Brandwagt, B.F., Mesbah, L.A., Takken, F.L., Laurent, P.L., Kneppers, T.J., Hille, J., and Nijkamp, H.J. (2000). A

437 longevity assurance gene homolog of tomato mediates resistance to *Alternaria alternata* f. sp. *lycopersici* toxins and

438 fumonisin B1. *Proc. Natl. Acad. Sci. USA.* 97: 4961–4966.

439

440 Brodersen, P., Petersen, M., Pike, H.M., Olszak, B., Skov, S., Oedum, N., Joergensen, L.B., Brown, R.E. and Mundy,

441 J. (2002). Knockout of *Arabidopsis* ACCELERATED CELL-DEATH11 encoding a sphingosine transfer protein

442 causes activation of programmed cell death and defense. *Genes & Development* 16, 490–502.

443

444 Chen, M. and Cahoon, E.B. (2009). Plant Sphingolipids: Structure, Synthesis and Function Lipids in Photosynthesis:

445 Essential and Regulatory Functions. pp. 77–115.

446

447 Dal'Molin C.G.D., Quek, L., Palfreyman, R.W., Brumbley, S.M. and Nielsen, L.K. (2010). AraGEM, a genome-scale

448 reconstruction of the primary metabolic network in *Arabidopsis*. *Plant Physiol.* 152, 579-589.

449

450 Delwiche, C.F. and Sharkey, T.D. (1993). Rapid appearance of <sup>13</sup>C in biogenic isoprene when <sup>13</sup>CO<sub>2</sub> is fed to intact

451 leaves. *Plant, Cell and Environment.* 16, 587-591.

452

453 Durner, J. and Klessig, D.F. (1995). Inhibition of ascorbate peroxidase by salicylic acid and 2,6-dichloroisonicotinic

454 acid, two inducers of plant defense responses. *Proc Natl Acad Sci USA.* 92, 11312–11316.

455

456 Durner, J. and Klessig, D.F. (1996). Salicylic acid is a modulator of tobacco and mammalian catalases. *J. Biol. Chem.*

457 271, 28492–28501.

458

459 Edwards, J.S. and Palsson, B.O. (2000). The *Escherichia coli* MG1655 *in silico* metabolic genotype: its definition,

460 characteristics, and capabilities. *Proc Natl Acad Sci USA.* 97, 5528-5533.

461

462 Edwards, J.S., Ibarra, R.U. and Palsson, B.O. (2001). *In silico* predictions of *Escherichia coli* metabolic capabilities

- 463 are consistent with experimental data. *Nat Biotechnol.* 19, 125-130.
- 464
- 465 Fiehn, O., Kopka, J., Dörmann, P., Altmann, T., Trethewey, R.N. and Willmitzer, L. (2000). Metabolite profiling for  
466 plant functional genomics. *Nat Biotechnol.* 18, 1157-1161.
- 467
- 468 Greenberg, J.T., Silverman, F.P. and Liang, H. (2000). Uncoupling salicylic acid dependent cell death and  
469 defense-related responses from disease resistance in the *Arabidopsis* mutant *acd5*. *Genetics.* 156, 341-350.
- 470
- 471 Hannun, Y.A. and Obeid, L.M. (2008). Principles of bioactive lipid signalling: lessons from sphingolipids. *Nat Rev.* 9,  
472 139-150.
- 473
- 474 Hasunuma, T., Harada, K., Miyazawa, S., Kondo, A., Fukusaki, E. and Miyake, C. (2010). Metabolic turnover  
475 analysis by a combination of *in vivo* <sup>13</sup>C-labelling from <sup>13</sup>CO<sub>2</sub> and metabolic profiling with CE-MS/MS reveals  
476 rate-limiting steps of the C<sub>3</sub> photosynthetic pathway in *Nicotiana tabacum* leaves. *J. Exp. Bot.* 61(4). 1041-1051.
- 477
- 478 Hucka, M., Finney, A., Sauro, H.M., Bolouri, H., Doyle, J.C., Kitano, H., Arkin, A.P., Bornstein, B.J., Bray, D., et al.  
479 (2003). The systems biology markup language (SBML): a medium for representation and exchange of biochemical  
480 network models. *Bioinformatics.* 19, 524-531.
- 481
- 482 Jones, J.D.G. and Dangl, J.L. (2006). The plant immune system. *Nature*, 444, 323-329.
- 483
- 484 Kanehisa M, Araki M, Goto S, Hattori M, Hirakawa M, Itoh M, Katayama T, Kawashima S, Okuda S, Tokimatsu T, et  
485 al (2008) KEGG for linking genomes to life and the environment. *Nucleic Acids Res.* 36: D480–D484
- 486
- 487 Keating, S.M., Bornstein, B.J., Finney, A. and Hucka, M. (2006). SBMLToolbox: an SBML toolbox for MATLAB  
488 users. *Bioinformatics.* 22, 1275-1277.
- 489
- 490 König, S., Feussner, K., Schwarz, M., Kaefer, A., Iven, T., Landesfeind, M., Ternes, P., Karlovsky, P., Lipka, V. and  
491 Feussner, I. (2012). *Arabidopsis* mutants of sphingolipid fatty acid α-hydroxylases accumulate ceramides and  
492 salicylates. *New Phytologist.* 196, 1086-1097.
- 493
- 494 Kruger, N.J., Masakapalli, S.K. and Ratcliffe, R.G. (2012). Strategies for investigating the plant metabolic network  
495 with steady-state metabolic flux analysis: lessons from an *Arabidopsis* cell culture and other systems. *J. Exp. Bot.* 63,  
496 2309-2323.
- 497
- 498 Lawton, K.A., Friedrich, L., Hunt, M., Weymann, K., Delaney, T., Kessmann, H., Staub, T. and Ryals, J. (1996).  
499 Benzothiadiazole induces disease resistance in *Arabidopsis* by activation of systemic acquired resistance signal  
500 transduction pathway. *Plant J.* 10, 71-82.
- 501
- 502 Liang, H., Yao, N., Song, J.T., Luo, S., Lu, H. and Greenberg, J.T. (2003). Ceramides modulate programmed cell

- 503 death in plants. *Genes & Development*. 17, 2636-2641.
- 504
- 505 Libourel, I.G.L. and Shachar-Hill, Y. (2008). Metabolic flux analysis in plants: from intelligent design to rational  
506 engineering. *Annu. Rev. Plant Biol.* 59, 625-650.
- 507
- 508 Lonien, J. and Schwender, J. (2009). Analysis of metabolic flux phenotypes for two *Arabidopsis* mutants with severe  
509 impairment in seed storage lipid synthesis. *Plant Physiol.* 151, 1617–1634.
- 510
- 511 Mahadevan, R., and Schilling, C.H. (2003). The effects of alternate optimal solutions in constraint-based  
512 genome-scale metabolic models. *Metab. Eng.* 5, 264–276.
- 513
- 514 Markham, J. E. and Jaworski, J. G. (2007). Rapid measurement of sphingolipids from *Arabidopsis thaliana* by  
515 reversed-phase high-performance liquid chromatography coupled to electrospray ionization tandem mass  
516 spectrometry. *Rapid Commun. Mass Spectrom.* 21(7), 1304-1314.
- 517
- 518 Markham, J.E., Lynch, D.V., Napier, J.A., Dunn, T.M. and Cahoon, E.B. (2013). Plant sphingolipids: function follows  
519 form. *Current Opinion in Plant Biology*. 16, 350–357.
- 520
- 521 Markham, J.E., Molino, D., Gissot, L., Bellec, Y., He ímaty, K., Marion, J., Belcram, K., Palauqui, J.C.,  
522 Satiat-JeuneMairêtre, B. and Faure, J.D. (2011). Sphingolipids containing very-long-chain fatty acids define a  
523 secretory pathway for specific polar plasma membrane protein targeting in *Arabidopsis*. *Plant Cell*. 23, 2362-2378.
- 524
- 525 Masakapalli, S.K., Le Lay, P., Huddleston, J.E., Pollock, N.L., Kruger, N.J. and Ratcliffe, R.G. (2010). Subcellular  
526 flux analysis of central metabolism in a heterotrophic *Arabidopsis* cell suspension using steady-state stable isotope  
527 labeling. *Plant Physiol.* 152, 602–619.
- 528
- 529 Meng, P.H., Raynaud, C., Tcherkez, G., Blanchet, S., Massoud, K., Domenichini, S., Henry, Y., ivine  
530 Soubigou-Taconnat, L., Lelarge-Trouverie, C., Saindrenan, P., Renou, J.P. and Bergounioux, C. (2009). Crosstalks  
531 between Myo-Inositol Metabolism, Programmed Cell Death and Basal Immunity in *Arabidopsis*. *PLoS ONE* 4(10),  
532 e7364.
- 533
- 534 Miura, K. and Tada, Y. (2014). Regulation of water, salinity, and cold stress responses by salicylic acid. *Front.Plant*  
535 *Sci.* 5, 4. doi:10.3389/fpls.2014.00004.
- 536
- 537 Moore, A.L., Albury, M.S., Crichton, P.G. and Affourtit, C. (2002). Function of the alternative oxidase: is it still a  
538 scavenger? *Trends in Plant Science*. 7, 478–481.
- 539
- 540 Mueller, L.A., Zhang, P. and Rhee, S.Y. (2003). AraCyc: A Biochemical Pathway Database for *Arabidopsis*. *Plant*  
541 *Physiol.* 132, 453-460.
- 542

- 543 Nöh, K. and Wiechert, W. (2006). Experimental design principles for isotopically instationary <sup>13</sup>C-labeling  
544 experiments. *Biotechnol. Bioeng.* 94, 234-251.
- 545
- 546 Nöh, K. and Wiechert, W. (2011). The benefits of being transient: isotope-based metabolic flux analysis at the short  
547 time scale. *Appl Microbiol Biotechnol.* 91, 1247-1265.
- 548
- 549 Noack S, Nöh K, Moch M, Oldiges M, Wiechert W (2010) Stationary versus non-stationary <sup>13</sup>C-MFA: a comparison  
550 using a consistent dataset. *J Biotechnol.* 154, 179-190.
- 551
- 552 Oberhardt, M.A., Goldberg, J.B., Hogardt, M. and Papin, J.A. (2010). Metabolic network analysis of *Pseudomonas*  
553 *aeruginosa* during chronic cystic fibrosis lung infection. *J. Bacteriol.* 192, 5534-5548.
- 554
- 555 Ozbayraktar, F.B.K. and Ulgen, K.O. (2011). Stoichiometric network reconstruction and analysis of yeast  
556 sphingolipid metabolism incorporating different states of hydroxylation. *BioSystems.* 104, 63-75.
- 557
- 558 Pata, M.O., Hannun, Y.A. and Ng, C.K. (2009). Plant sphingolipids: decoding the enigma of the Sphinx. *New*  
559 *Phytologist.* 185, 611–630.
- 560
- 561 Poolman, M.G., Miguet, L., Sweetlove, L.J. and Fell, D.A. (2009). A genome-scale metabolic model of *Arabidopsis*  
562 and some of its properties. *Plant Physiol.* 151, 1570-1581.
- 563
- 564 Radrich, K., Tsuruoka, Y., Dobson, P., Gevorgyan, A., Swainston, N., Baart, G. and Schwartz, J.M. (2010).  
565 Integration of metabolic databases for the reconstruction of genome-scale metabolic networks. *BMC Syst. Biol.* 4, 114.  
566 doi: 10.1186/1752-0509-4-114.
- 567
- 568 Reed, J.L. and Palsson, B.O. (2003). Thirteen years of building constraint based *in silico* models of *Escherichia coli*.  
569 *J. Bacteriol.* 185, 2692-2699.
- 570
- 571 Ryan PR, Liu Q, Sperling P, Dong B, Franke S and Delhaize E (2007) A higher plant delta8 sphingolipid desaturase  
572 with a preference for (Z)-isomer formation confers aluminum tolerance to yeast and plants. *Plant Physiol.* 144:  
573 1968-1977.
- 574
- 575 Saucedo-Garcia, M., Guevara-Garcia, A., Gonzalez-Solis, A., Cruz-Garcia, F., Vazquez-Santana, S., Markham, J.E.,  
576 Lozano-Rosas, M.G., Dietrich, C.R., Ramos-Vega, M., Cahoon, E.B. and Gavilanes-Ruiz, M. (2011). MPK6,  
577 sphinganine and the LCB2a gene from serine palmitoyltransferase are required in the signaling pathway that mediates  
578 cell death induced by long chain bases in *Arabidopsis*. *New Phytologist.* 191, 943-957.
- 579
- 580 Schellenberger, J., Que, R., Fleming, R.M., Thiele, I., Orth, J.D., Feist, A.M., Zielinski, D.C., Bordbar, A., Lewis,  
581 N.E., Rahmanian, S., Kang, J., Hyduke, D.R. and Palsson, B.Ø. (2011). Quantitative prediction of cellular  
582 metabolism with constraint-based models: the COBRA Toolbox v2.0. *Nat Protoc.* 6, 1290-1307.



- 583
- 584 Schmidt, H. and Jirstrand, M. (2006). Systems Biology Toolbox for MATLAB: a computational platform for research  
585 in systems biology. *Bioinformatics*. 22, 514-515.
- 586
- 587 Seaver, S.M.D., Henry, C.S. and Hanson, A.D. (2012). Frontiers in metabolic reconstruction and modeling of plant  
588 genomes. *J. Exp. Bot.* 63, 2247-2258.
- 589
- 590 Shastri, A.A. and Morgan, J.A. (2007). A transient isotopic labeling methodology for <sup>13</sup>C metabolic flux analysis of  
591 photoautotrophic microorganisms. *Phytochemistry*. 68, 2302-2312.
- 592
- 593 Shimono, M., Sugano, S., Nakayama, A., Jiang, C.J., Ono, K., Toki, S. and Takatsuji, H. (2007). Rice WRKY45 plays  
594 a crucial role in benzothiadiazole-inducible blast resistance. *Plant Cell*. 19, 2064-2076.
- 595
- 596 Slaymaker, D.H., Navarre, D.A., Clark, D., del Pozo, O., Martin, G.B. and Klessig, D.F. (2002). The tobacco salicylic  
597 acid-binding protein 3 (SABP3) is the chloroplast carbonic anhydrase, which exhibits antioxidant capacity and plays  
598 a role in the hypersensitive response. *Proc. Natl Acad. of Sci., USA*. 99, 11640-11645.
- 599
- 600 Smith, A. M. and Stitt, M. (2007). Coordination of carbon supply and plant growth. *Plant Cell Environ.* 30,  
601 1126-1149.
- 602
- 603 Sperling P, Zahringer U. and Heinz E (1998) A sphingolipid desaturase from higher plants. Identification of a new  
604 cytochrome b5 fusion protein. *J Biol Chem* 273: 28590-28596.
- 605
- 606 Spoel, S.H. and Dong, X.N. (2012). How do plants achieve immunity? Defence without specialized immune cells.  
607 *Nat Rev Immunol*. 12, 89-100.
- 608
- 609 Stitt, M., Sulpice, R. and Keurentjes, J. (2010). Metabolic networks: how to identify key components in the  
610 regulation of metabolism and growth. *Plant Physiol*. 152, 428-444.
- 611
- 612 Sweetlove, L.J and Ratcliffe, R.G. (2011). Flux-balance modeling of plant metabolism. *Front. Plant Sci.* 2:38.  
613 doi:10.3389/fpls.2011.00038
- 614
- 615 Ternes, P., Feussner, K., Werner, S., Lerche, J., Iven, T., Heilmann, I., Riezman, H., and Feussner, I. (2011).  
616 Disruption of the ceramide synthase LOH1 causes spontaneous cell death in *Arabidopsis thaliana*. *New Phytol* 192:  
617 841-854.
- 618
- 619 Thiele, I. and Palsson, B.O. (2010). A protocol for generating a high-quality genome-scale metabolic reconstruction.  
620 *Nat protocol*. 5, 93-121.
- 621
- 622 van Leeuwen, H., Kliebenstein, D.J., West, M.A., Kim, K., van Poecke, R., Katagiri, F., Michelmore, R.W., Doerge

- 623 R.W. and St Clair, D.A. (2007). Natural variation among *Arabidopsis thaliana* accessions for transcriptome response  
624 to exogenous salicylic acid. *Plant Cell* 19, 2099–2110.
- 625
- 626 Varma, A. and Palsson, B.O. (1994). Metabolic flux balancing: basic concepts, scientific and practical use. *Nat*  
627 *Biotechnol.* 12, 994-998.
- 628
- 629 Vicente, M.R. and Plasencia, J. (2011). Salicylic acid beyond defence: its role in plant growth and development. *J*  
630 *Exp Bot.* 62, 3321-3338.
- 631
- 632 Vlot, A.C., Dempsey, D.A. and Klessig, D.F. (2009). Salicylic acid, a multifaceted hormone to combat disease. *Annu*  
633 *Rev Phytopathol.* 47, 177-206.
- 634
- 635 Wang, D., Amornsiripanitch, N. and Dong, X.N. (2006). A genomic approach to identify regulatory nodes in the  
636 transcriptional network of systemic acquired resistance in plants. *PLoS Pathogens.* 2, 1042-1050.
- 637
- 638 Wang, W.M., Yang, X.H., Tangchaiburana, S., Ndeh, R., Markham, J.E., Tsegaye, Y., Dunn, T.M., Wang, G.L.,  
639 Bellizzi, M., Parsons, J.F., Morrissey, D., Bravo, J.E., Lynch, D.V. and Xiao, S.Y. (2008). An  
640 Inositolphosphorylceramide Synthase Is Involved in Regulation of Plant Programmed Cell Death Associated with  
641 Defense in *Arabidopsis*. *Plant Cell.* 20, 3163–3179.
- 642
- 643 Welti, R., Li, W., Li, M., Sang, Y., Biesiada, H., Zhou, H., Rajashekar, C.B., Williams, T.D. and Wang, X. (2002).  
644 Profiling membrane lipids in plant stress responses. *J Bio. Chem.* 277, 31194-32002.
- 645
- 646 Wiechert, W. and Nöh, K. (2005). From stationary to instationary metabolic flux analysis. *Adv Biochem Eng*  
647 *Biotechnol.* 92, 145-172.
- 648
- 649 Yan, S.P. and Dong, X.N. (2014). Perception of the plant immune signal salicylic acid. *Current Opinion in Plant*  
650 *Biology.* 20, 64–68.
- 651
- 652 Yoshimoto, K., Hanaoka, H., Sato, S., Kato, T., Tabata, S., Noda, T. and Ohsumi, Y. (2004). Processing of ATG8s,  
653 ubiquitin-like proteins, and their deconjugation by ATG4s are essential for plant autophagy. *Plant Cell.* 16,  
654 2967-2983.
- 655

656 **Figure Legends**

657

658 **Figure 1.**  $^{15}\text{N}$  incorporation curves for sphingolipid species.

659 Ten-day-old wild-type seedlings were transferred to 5 mM  $^{15}\text{N}$ - serine labeled N-deficient 1/2x  
660 MS liquid medium for the indicated times. Sphingolipids were then extracted and measured as  
661 described in Methods. The  $^{15}\text{N}$  fraction incorporation curve was calculated based on the formula  
662 shown in Methods. Error bars represent the means  $\pm$ SE from triplicate biological repeats. The  
663 measured sphingolipid species were: ceramide (A), hydroxyceramide (B), glucosylceramide (C)  
664 and LCB (D). LCB and fatty acid in ceramide species represent: LCB; d/t (di/trihydroxy) 18 (18  
665 carbon chain): 1 (one desaturation) followed by fatty acid; c/h/g (non-hydroxyl / hydroxyl /  
666 glucosyl and hydroxyl) 24 (24 carbon chain): 0 (no desaturations).

667

668 **Figure 2.** Simulated flux distribution of selected sphingolipid species.

669 The untreated plants (black) and *in silico* SA (light gray) and BTH-treated plants (gray) were  
670 taken from the flux balance model. The effects of exogenous SA and BTH were simulated by  
671 changing the target flux bound proportional to its related gene expression alteration identified by  
672 published microarray data (Wang *et al.*, 2006; van Leeuwen *et al.*, 2007). LC, long-chain ( $\leq$ C18);  
673 VLC: very-long-chain ( $>$ C18).

674

675

676 **Figure 3.** Flux variations among selected reactions of different sphingolipid species under no  
677 treatment or *in silico* SA or BTH treatments. LCB fluxes are omitted for their too large flux  
678 variation up to 1000 nmol/g/h, while other fluxes keep rigid after *in silico* treatment (see  
679 supplemental Table S3).

680

681 **Table 1.** Overview of sphingolipid species in the FBA model.

682

Symbol	Sphingolipid species	Pool size (nmol·g <sup>-1</sup> )	Stoichiometry in objective function
d18:0 LCB	Long-chain base	1.686182	0.050201
d18:1 LCB	Long-chain base	0.323814	0.017119
t18:0 LCB	Long-chain base	2.243848	0.044619
t18:1 LCB	Long-chain base	0.894187	8.05E-05
t18:1 c16:0	long-chain ceramide	1.375136	0.14095
t18:0 c16:0	long-chain ceramide	0.078273	0.006289
d18:1 c16:0	long-chain ceramide	0.103578	0.017411
d18:0 c16:0	long-chain ceramide	0.323513	0.040446
t18:0 c24:0	very-long-chain ceramide	17.51997	0.47712
t18:1 c24:0	very-long-chain ceramide	30.1346	0.775466
t18:0 c24:1	very-long-chain ceramide	4.702168	0.119545
t18:1 c24:1	very-long-chain ceramide	10.12495	0.344293
t18:0 c26:0	very-long-chain ceramide	5.964148	0.129493
t18:1 c26:0	very-long-chain ceramide	29.47465	0.671015
t18:0 c26:1	very-long-chain ceramide	0.326354	0.005744
t18:1 c26:1	very-long-chain ceramide	6.565916	0.208064
t18:1 h160	long-chain hydroxyceramide	6.406314	0.154383
t18:0 h160	long-chain hydroxyceramide	0.682043	0.012748
d18:1 h16:0	long-chain hydroxyceramide	0.351323	0.020931
d18:0 h16:0	long-chain hydroxyceramide	0.292355	0.019623
t18:0 h24:0	very-long-chain hydroxyceramide	10.38919	0.01712
t18:1 h24:0	very-long-chain hydroxyceramide	80.91966	1.148618
t18:0 h24:1	very-long-chain hydroxyceramide	8.615409	0.124845
t18:1 h24:1	very-long-chain hydroxyceramide	0.169527	1.53E-05
t18:0 h26:0	very-long-chain hydroxyceramide	3.30798	0.003149
t18:1 h26:0	very-long-chain hydroxyceramide	17.71101	0.218833
t18:0 h26:1	very-long-chain hydroxyceramide	1.005991	9.05E-05
t18:1 h26:1	very-long-chain hydroxyceramide	10.14596	0.27478
t18:1 h16:0	long-chain glucosylceramide	7.336978	0.03589
t18:0 h16:0	long-chain glucosylceramide	0.00001	9.00E-10
d18:1 h16:0	long-chain glucosylceramide	23.26684	0.177984
d18:0 h16:0	long-chain glucosylceramide	0.191598	0.001506
t18:0 h24:0	very-long-chain glucosylceramide	1.55239	0.00014
t18:1 h24:0	very-long-chain glucosylceramide	14.59155	0.055296
t18:0 h24:1	very-long-chain glucosylceramide	0.00001	9.00E-10
t18:1 h24:1	very-long-chain glucosylceramide	17.28822	0.057862
t18:0 h26:0	very-long-chain glucosylceramide	0.00001	9.00E-10
t18:1 h26:0	very-long-chain glucosylceramide	8.470761	0.032563
t18:0 h26:1	very-long-chain glucosylceramide	0.00001	9.00E-10
t18:1 h26:1	very-long-chain glucosylceramide	5.706558	0.016164

683

684

685 **Table 2.** Isotopic incorporation rate for major sphingolipids, with or without 100  $\mu$ M SA or 100  $\mu$ M BTH treatments  
686

Symbol	Sphingolipid species	Isotope	Isotope	Isotope
		incorporation rate (nmol·g <sup>-1</sup> ·h <sup>-1</sup> ) untreated	incorporation rate (nmol·g <sup>-1</sup> ·h <sup>-1</sup> ) SA-treated	incorporation rate (nmol·g <sup>-1</sup> ·h <sup>-1</sup> ) BTH-treated
d18:0 LCB	Long-chain base	0.062022	0.055779	0.038494*
d18:1 LCB	Long-chain base	0.005016	0.059469*	0.031829*
t18:0 LCB	Long-chain base	0.030297	0.049577	0.023784
t18:1 LCB	Long-chain base	1.43E-02	8.94E-06*	5.44E-04*
t18:1 c16:0	long-chain ceramide	0.100845	0.241159*	0.221878*
d18:0 c16:0	long-chain ceramide	0.04256	0.066754*	0.0477
t18:0 c24:0	very-long-chain ceramide	0.386836	0.495358	0.505011*
t18:1 c24:0	very-long-chain ceramide	0.418402	0.60068*	0.538219
t18:0 c24:1	very-long-chain ceramide	0.217738	0.144568*	0.176221
t18:1 c24:1	very-long-chain ceramide	0.485274	0.500902	0.547493
t18:0 c26:0	very-long-chain ceramide	0.049354	0.048909	0.031827
t18:1 c26:0	very-long-chain ceramide	0.136971	0.179349	0.184011*
t18:1 c26:1	very-long-chain ceramide	3.44E-02	5.44E-02*	6.98E-02*
t18:1 h16:0	long-chain hydroxyceramide	0.268339	0.253601	0.177361*
t18:1 h24:0	very-long-chain hydroxyceramide	1.25246	1.139387	0.965043
t18:0 h24:1	very-long-chain hydroxyceramide	0.092809	0.13231	0.167954*
t18:1 h26:0	very-long-chain hydroxyceramide	0.157256	0.200213*	0.183134
t18:1 h26:1	very-long-chain hydroxyceramide	1.86E-01	1.06E-01*	1.29E-01
d18:1 h16:0	long-chain glucosylceramide	0.142007	0.126636	0.199323*
t18:1 h24:0	very-long-chain glucosylceramide	0.076921	0.13433*	0.265554*
t18:1 h24:1	very-long-chain glucosylceramide	0.073858	0.076487	0.15701*
t18:1 h26:0	very-long-chain glucosylceramide	0.040668	0.053585	0.060641*

687 \* indicate significant change (P<0.05, FDR<0.05 in multiple covariance analysis) of incorporation rate compared to  
688 untreated plants.

689

690

691

692

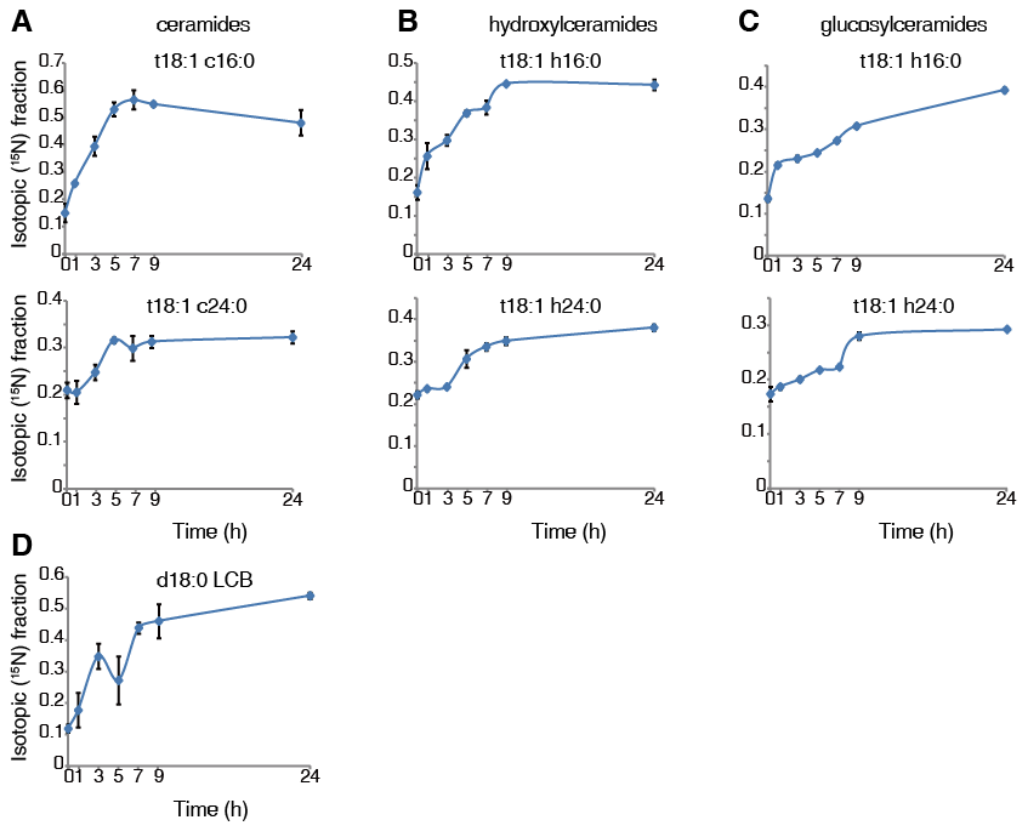


**Figure 1.**  $^{15}\text{N}$  incorporation curve for sphingolipid species.

Ten-day-old wild-type seedlings were transferred to 5 mM  $^{15}\text{N}$ -serine labeled N-deficient 1/2x MS liquid medium for the indicated times. Sphingolipids were then extracted and measured as described in Methods. The  $^{15}\text{N}$  fraction incorporation curve was calculated based on the formula shown in Methods. Error bars represent the means  $\pm$ SE from triplicate biological repeats. The measured sphingolipid species were: ceramide (A), hydroxylceramide (B), glucosylceramide (C) and LCB (D). LCB and fatty acid in ceramide species represent: LCB; d/t (di/trihydroxy) 18 (18 carbon chain): 1 (one desaturation) followed by fatty acid; c/h/g (non-hydroxyl/ hydroxyl / glucosyl and hydroxyl) 24 (24 carbon chain): 0 (nodesaturations).

693

694

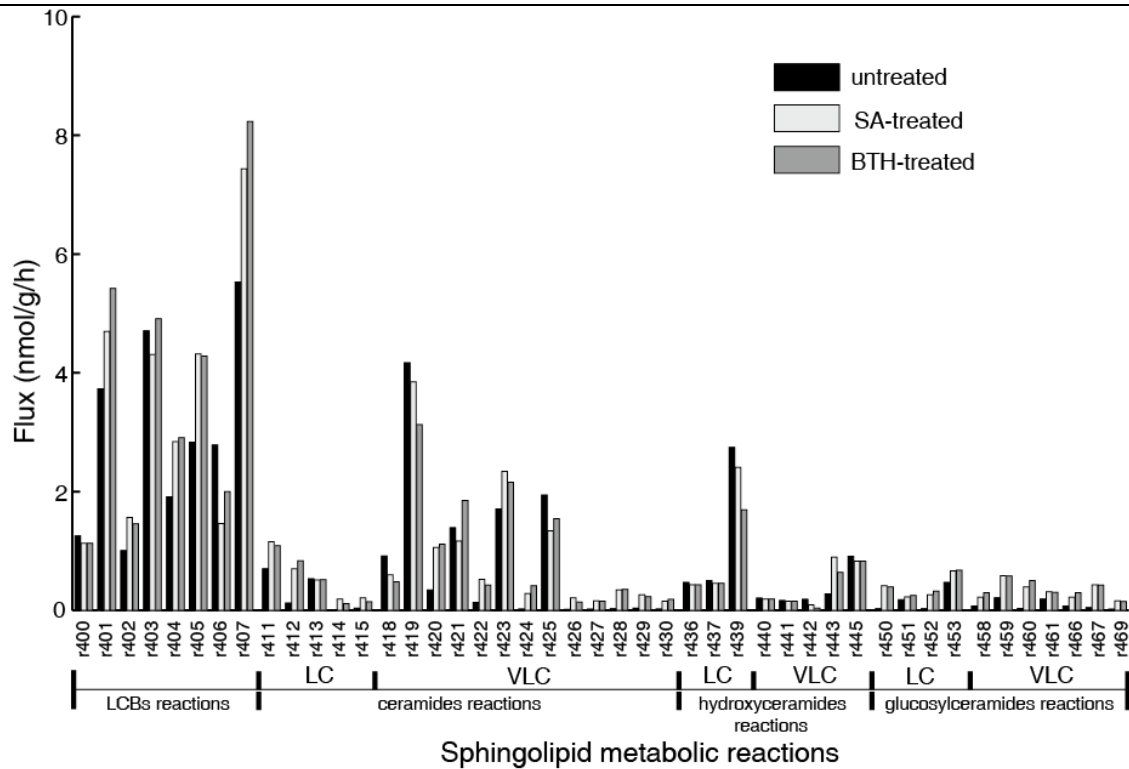


**Figure 2.** Simulated flux distribution of selected sphingolipid species.

The untreated plants (black) and *in silico* SA (light gray) and BTH-treated plants (gray) were taken from the flux balance model. The effects of exogenous SA and BTH were simulated by changing the target flux bound proportional to its related gene expression alteration identified by published microarray data (Wang *et al.*, 2006; van Leeuwen *et al.*, 2007). LC, long-chain ( $\leq C18$ ); VLC: very-long-chain ( $> C18$ ).

695  
696

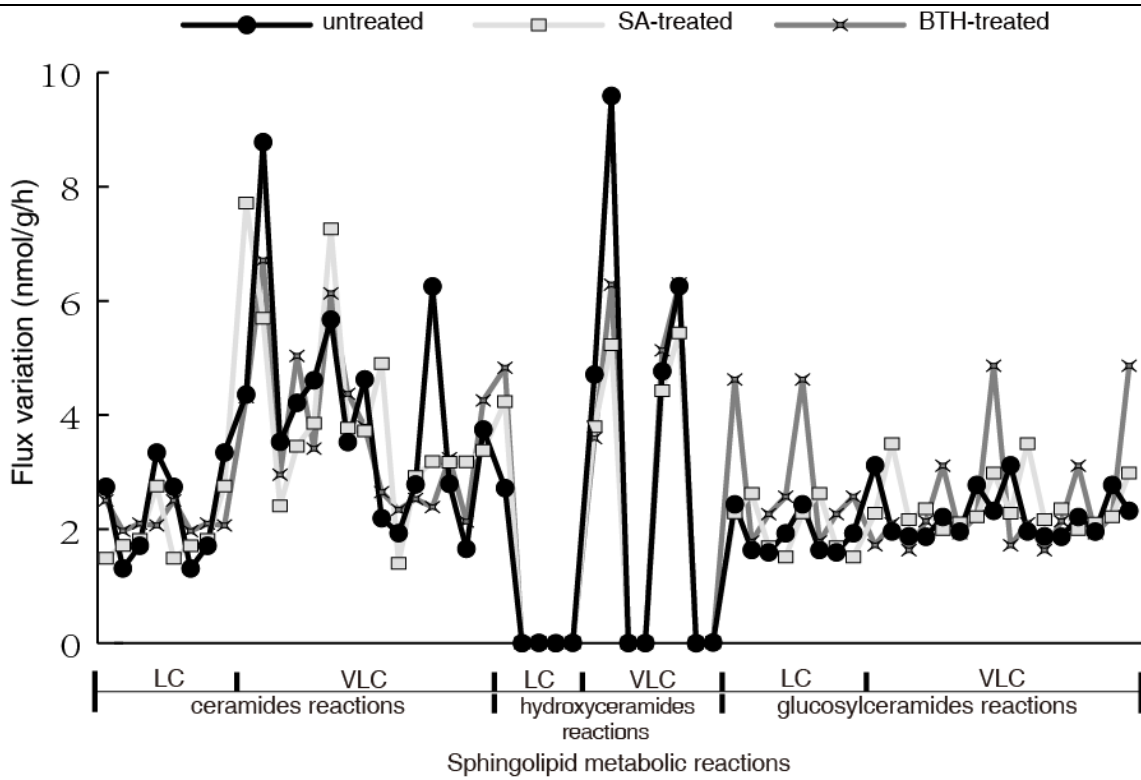


**Figure 3.** Flux variations among selected reactions of different spingolipid species under no treatment or *in silico* SA or BTH treatments. LCB fluxes are omitted for their too large flux variation up to 1000 nmol/g/h, while other fluxes keep rigid after *in silico* treatment (see supplemental Table S3).

697  
698